

**NASA TECHNICAL  
MEMORANDUM**

**N 68 34 09 1**  
**NASA TM X-52441**

**NASA TM X-52441**

**EXPERIMENTAL AND ANALYTICAL INVESTIGATION OF THE DYNAMIC  
RESPONSE OF A SUPERSONIC MIXED-COMPRESSION INLET**

by Joseph F. Wasserbauer and Ross G. Willoh  
Lewis Research Center  
Cleveland, Ohio

TECHNICAL PAPER proposed for presentation at Fourth  
Propulsion Joint Specialist Conference sponsored by the  
American Institute of Aeronautics and Astronautics  
Cleveland, Ohio, June 10-14, 1968

**NATIONAL AERONAUTICS AND SPACE ADMINISTRATION · WASHINGTON, D.C. · 1968**

**EXPERIMENTAL AND ANALYTICAL INVESTIGATION OF THE DYNAMIC RESPONSE  
OF A SUPERSONIC MIXED-COMPRESSION INLET**

**by Joseph F. Wasserbauer and Ross G. Willoh**

**Lewis Research Center  
Cleveland, Ohio**

**TECHNICAL PAPER proposed for presentation at**

**Fourth Propulsion Joint Specialist Conference  
sponsored by the American Institute of Aeronautics and Astronautics  
Cleveland, Ohio, June 10-14, 1968**

**NATIONAL AERONAUTICS AND SPACE ADMINISTRATION**

# EXPERIMENTAL AND ANALYTICAL INVESTIGATION OF THE DYNAMIC RESPONSE OF A SUPERSONIC MIXED-COMPRESSION INLET

by Joseph F. Wasserbauer and Ross G. Willoh

Lewis Research Center  
National Aeronautics and Space Administration  
Cleveland, Ohio

## Introduction

Proper design of inlet control systems requires thorough knowledge of the dynamic characteristics of the inlet and, in particular, the dynamic response of the terminal shock to both internal and external disturbances. The inlet dynamic characteristics can be obtained either experimentally or by means of analytical simulation.

Experimentally, data from dynamic studies of mixed-compression and external compression inlets have been, in general, limited to disturbance frequencies below 50 Hz. However, in a recent investigation,<sup>(1)</sup> the disturbance frequency was extended to 200 Hz. The results of this investigation revealed that a resonant condition occurred in the dynamic response of this inlet at about 90 Hz. The dynamic characteristics were obtained only for a cold flow model with large internal volume. Ideally, the dynamic response of an inlet coupled to an operating turbojet engine should also be experimentally determined.

A test was subsequently conducted in the Lewis 10-by-10 Foot Supersonic Wind Tunnel and experimental data were obtained for an isolated inlet coupled to short and long cold-flow pipe configurations and also for the inlet coupled to an operating turbojet engine. The isolated inlet and the inlet-engine configurations were subjected to an internal disturbance at frequencies up to 240 Hz and also to an external disturbance at frequencies up to 15 Hz. Data were also obtained for the inlet with and without boundary layer bleed in the throat region.

A mathematical description of the inlet dynamic behavior is also briefly presented. The analysis combines a linearized set of equations across the shock with a relatively exact solution of the subsonic duct wave equations. The solutions for the wave equations are written in terms of time shifts and then expressed in the frequency domain. Data from a digital computer solution of the equations for the inlet frequency response are presented. The complete analysis is presented in Ref. 2. A comparison between the experimental and analytical results is made.

## Apparatus and Procedure

The experimental investigation was conducted in the Lewis 10-by-10 Foot Supersonic Wind Tunnel at a free stream Mach number of 2.5. An isometric view of the inlet is shown in Fig. 1(a). The inlet was designed for Mach number 2.5 operation with an inlet cowl lip diameter of 0.465 meter and with 60 percent of the total supersonic area contraction ratio occurring internally. The inlet matched the airflow requirements of a J-85-13

turbojet engine. Boundary layer bleed on the cowl and centerbody were provided in the inlet throat region. A detailed description of the inlet steady state aerodynamic performance is reported in Ref. 3.

Internal and external disturbance devices were used to perturb the inlet flow. The internal disturbance devices generated symmetrical and unsymmetrical flow perturbations. The symmetrical disturbance was obtained by sinusoidally oscillating three of the six inlet bypass doors at frequencies up to 140 Hz. The locations of the hydraulically operated bypass doors are shown on Figs. 1(a) and (b). The unsymmetrical disturbance was obtained from a rotary valve positioned in place of one bypass door, Fig. 1(b). The valve exit area was designed to vary sinusoidally during constant speed rotation. The external disturbance was a trapezoidal gust generator plate positioned above and upstream of the inlet and oscillated through 1° of arc at frequencies up to 15 Hz, Fig. 1(b). Construction and operation of the rotary valve and gust generator plate is described in Ref. 1.

The inlet shock position dynamics were obtained from eight static pressure transducers located in the inlet throat, Fig. 1(a). The analog signal of each transducer indicated the time of shock crossing. The times at which the shock crossed the various transducer positions was then used with the method of least mean square to obtain amplitude and phase shift of the shock position dynamics<sup>(1)</sup>. The response of the throat exit static pressure was recorded on analog tape by a transducer shown in Fig. 1(a). Calibration of the tube-transducer assembly allowed for correction of the pressure fluctuation signals due to tube assembly dynamics.

Experimental data for the external and internal disturbances were obtained for the inlet coupled to short and long cold pipe configurations and also for the inlet coupled to an operating turbojet engine. The short and long cold pipe configurations had the internal flow choked at the diffuser exit and 2.36 meters further downstream at the model exit station, respectively. In addition to these configurations, dynamic data were also obtained with and without boundary layer bleed in the inlet throat region.

The dynamic responses presented in the figures are in terms of amplitude ratio and phase shift. The amplitude ratio is defined as the amplitude at the test frequency divided by the amplitude at a frequency of 1 Hz.

Faired curves rather than data points are presented on Figs. 2, 4, 5, and 6 so that the comparisons between the different inlet configurations can be made easily. The data points are presented on Figs. 3, 9, 10, and 11.

## Experimental Results

### Internal Disturbances

The dynamic responses of shock position to a symmetrical internal disturbance for the three inlet configurations are presented in Fig. 2. For these configurations, the inlet throat region had normal boundary layer bleed on the cowl and centerbody. The ratio of the change in shock position to the change in weight flow ( $\Delta X_S/\Delta \dot{w}$ ) was about 0.122 meter per kilogram per second at the reference frequency of 1 Hz. The disturbance amplitude was  $\pm 0.40$  kg/sec for the cold flow configurations and  $\pm 0.30$  kg/sec for the inlet-engine configuration. The maximum capture inlet flow rate was 12.90 kg/sec.

All three configurations exhibited a resonant condition at about 50 to 55 Hz. Little or no change in resonant frequency was noted when the location of the internal flow choke point was changed and when the engine was coupled to the inlet. The shock position dynamics for the choked diffuser exit configuration and the inlet-engine configuration showed minor differences except in the vicinity of 30 Hz. Increasing the diffuser volume decreased the magnitude of the amplitude ratio more rapidly at lower frequencies and accentuated the resonant condition as indicated by the solid curve. First-order lumped parameter analyses, such as reported in Ref. 4, predict the data to about 25 or 30 Hz. However, this type of analysis cannot predict resonances such as those observed in this test.

The variation in phase shift with disturbance frequency appeared to be similar for the choked diffuser exit and the inlet-engine configuration. The phase shift for the configuration with the model exit choked decreased more rapidly at low frequencies but a leading effect is noticed just prior to the resonant frequency. At the higher frequencies the phase shifts appear to be similar for all three configurations.

The dynamic response of shock position to an unsymmetrical internal disturbance is presented for frequencies up to 240 Hz, Fig. 3. The internal flow was choked at the model exit for this configuration. The data presented here are for amplitude ratio only and were obtained by the inlet unstart method described in Ref. 1. The incremental change in weight flow through the rotary valve was constant at about  $\pm 0.13$  kg/sec over the entire frequency range.

The location of the shock position at unstart is upstream of its normal location in the inlet throat where the usual shock position response data are taken. This difference plus the unsymmetrical nature of the internal disturbance could cause the differences in response noted in comparison of this data to that presented in Fig. 2 for the same configuration. Resonant conditions appear at about 60, 125, and 210 Hz. The magnitude of the amplitude ratio at the resonant condition of 60 Hz was equal to the magnitude at 1 Hz.

Although the resonant conditions were at frequencies greater than 40 Hz, the test model under consideration was of moderate size (0.465 meter cowl lip diameter)

and therefore the resonant frequencies should be reduced by a scale factor for comparison with larger models. By limiting the permissible gain for a stable control system, the presence of these resonances can affect controlled system performance at relatively low frequencies.

Figure 4 presents a comparison of the dynamic responses of shock position and throat exit static pressure for a downstream symmetrical internal disturbance in the inlet-engine configuration. At the reference frequency of 1 Hz, the change in static pressure at the throat exit was  $6.89 \times 10^3$  newton per square meter for the corresponding change of 0.59 kg/sec in the bypass weight flow.

In general, the dynamic response of static pressure just downstream of the inlet throat should lead the shock position dynamics in a first order manner. Similar values in amplitude ratio were noted for the two response curves to a frequency of about 70 Hz, and the two responses are within a factor of 0.707 to frequencies beyond 90 Hz indicating a first order corner frequency larger than 90 Hz.

Comparison of the two response curves in phase shift (dashed and solid curves) shows a larger difference than would be expected from a first-order relationship whose corner frequency is larger than 90 Hz. However, consideration of the dead time between the average shock location in the throat and the throat exit static tap (15 cm downstream) shows that the difference in phase shift of the two responses (dashed and broken curves) to be less than  $45^\circ$  for frequencies beyond 90 Hz. The analysis presented later in this report predicts the corner frequency to be about 120 Hz.

The effect of inlet throat bleed on shock position dynamics for the inlet-engine configuration is presented in Fig. 5. The resonant frequency was reduced from 55 Hz to approximately 40 Hz when the downstream throat bleed was sealed. The ratio of the change in shock position to change in bypass weight flow ( $\Delta X_S/\Delta \dot{w}$ ) for the inlet with the downstream throat bleed sealed was 4.4 times the ( $\Delta X_S/\Delta \dot{w}$ ) for the inlet with full throat bleed at 1 Hz. Therefore, the terminal shock of the inlet with sealed bleed was more sensitive to small downstream disturbances while for the inlet with the full throat bleed, the terminal shock was less sensitive but subject to a more pronounced resonant condition. Small differences in the phase shifts of the two configurations were noted with the phase of the sealed bleed configuration lagging that of the full bleed configuration.

### External Disturbance

The response of shock position to an external disturbance for the inlet-engine configuration with the downstream throat bleed sealed is presented in Fig. 6. The ratio of the change in shock position to change in gust plate angle of attack ( $\Delta X_S/\Delta \phi$ ) was 0.070 meter per degree. The external disturbance perturbed the flow in both the supersonic and subsonic portions of the duct. The gust plate produced simultaneous changes in free stream Mach number and flow angle of attack in the flow field ahead of the inlet.

The data of Fig. 6 indicates a moderate reduction in the amplitude ratio to about 10 Hz. From 10 to 15 Hz the response in amplitude was flat or slightly increasing in magnitude. This would suggest that a possible lead component in the amplitude ratio may have been present after 15 Hz. Little difference in phase shift was noted for the two test conditions over the range of test frequencies. In Ref. 1, inlet response data resulting from an external disturbance indicated a lead characteristic in both amplitude ratio and phase shift causing the inlet to be sensitive to higher frequency external disturbances.

### Analytical Results

The one dimensional mathematical analysis of shock position dynamics in a mixed compression inlet can be conveniently subdivided into two problems. First the interaction of shock position with adjacent variables and, secondly, the subsonic duct analysis. Figure 7 shows the idealized inlet considered in the analysis. The inlet was treated mathematically as a duct with varying area followed by a duct with constant area. The upstream end of the duct is bounded by a moving normal shock and the downstream end by a fixed choke station.

The analytical results here presented are based on a linearized set of equations across the normal shock combined with linearized wave equations for the subsonic duct. The linearized wave equations can be integrated only over a constant area section. The diverging portion of the subsonic diffuser is thus mathematically represented as three constant area sections.

Previous dynamic analyses of inlets have applied various techniques to the problem. Reference 5 presents a detailed analysis of the lumped volume Helmholtz resonator concept. This representation, however, does not predict the repeated resonances typical of a distributed parameter system. The analysis applied in this paper does predict such resonances without being significantly more complicated in application than the Helmholtz-resonator concept. Efforts have also been directed toward the application of the method of characteristics to the problem. This technique should provide accurate results but with a significant increase in computation time and analytical complexity.

The linearized equations used in this analysis can provide a closed form solution for each section and when combined yield an easily calculated frequency response. It is also possible to program the equations in a simulation language such as Mimic or on an analog computer for direct control system simulation.

The equations for both shock motion and the subsonic duct are written with flow, total pressure, and entropy as the dependent system variables. These parameters have the advantage of being constant in the steady state, and thus considerably simplify the small perturbation analysis. A more thorough development of the analysis is presented in Ref. 2. Mass, momentum, and energy balances taken across a normal shock can be modified to account for shock motion. With the assumption of perfect gas relations and negligible changes in

duct area across the shock, a linearized set of equations is presented. Restricting consideration to disturbances originating downstream of the normal shock, the dynamic relations of equations (1) are derived:

$$\left. \begin{aligned} \tilde{P}_2 &= -C_1 \left[ L_T \frac{A'}{A} + C_2 s \right] \tilde{X}_s \\ \tilde{w}_2 &= C_3 s \tilde{X}_s \\ \tilde{S}_2 &= C_1 \left[ L_T \frac{A'}{A} - C_3 s \right] \tilde{X}_s \end{aligned} \right\} \quad (1)$$

where

$$C_1 = \frac{7(M_1^2 - 1)}{(7M_1^2 - 1)}$$

$$C_2 = \frac{5(1 + 0.2M_1^2)^{1/2}}{6a_{T_1} M_1} L_T$$

and

$$C_3 = \frac{1}{a_{T_1} M_1} \frac{(M_1^2 - 1)}{(1 + 0.2M_1^2)^{1/2}} L_T$$

and a  $\sim$  over a quantity designates a small perturbation variable, that is,  $\tilde{P} = \Delta P_T / P_T$ ,  $\tilde{w} = \Delta \dot{w} / \dot{w}$ , and  $\tilde{S} = \Delta S / R$ .

In Ref. 2 the conventional compressible flow continuity, momentum, and energy equations for quasi-one dimensional flow are formulated as wave equations in terms of the chosen system variables total pressure, flow, and entropy. With the assumption of invicid, non-heat conducting flow of an ideal gas it is shown that:

$$\left. \begin{aligned} \frac{g}{a\rho_T} \frac{\delta^+ P_T}{\delta t} + \frac{1}{A\rho} \frac{\delta^+ \dot{w}}{\delta t} + \frac{aM(M+2)}{7R} \frac{\delta^+ S}{\delta t} &= 0 \\ \frac{g}{a\rho_T} \frac{\delta^- P_T}{\delta t} - \frac{1}{A\rho} \frac{\delta^- \dot{w}}{\delta t} - \frac{aM(2-M)}{7R} \frac{\delta^- S}{\delta t} &= 0 \\ \frac{\delta S}{\delta t} + v \frac{\delta S}{\delta x} &= 0 \end{aligned} \right\} \quad (2)$$

where

$$\frac{\delta^+}{\delta t} = \frac{\delta}{\delta t} + (v+a) \frac{\delta}{\delta x}$$

$$\frac{\delta^-}{\delta t} = \frac{\delta}{\delta t} + (v-a) \frac{\delta}{\delta x}$$

The above equations are then linearized for small perturbations about a steady flow condition and with the substitution of:

$$\alpha = \frac{7M}{(M^2 + 5)}$$

$$\beta = \frac{M(M+2)}{(M^2 + 5)}$$

and

$$\gamma = \frac{M(2-M)}{(M^2 + 5)}$$

equations (2) become:

$$\left. \begin{aligned} \left[ \frac{\delta}{\delta t} + (v+a) \frac{\delta}{\delta x} \right] \left[ \tilde{P}_T + \alpha \tilde{w} + \beta \tilde{S} \right] &= 0 \\ \left[ \frac{\delta}{\delta t} + (v-a) \frac{\delta}{\delta x} \right] \left[ \tilde{P}_T + \alpha \tilde{w} - \gamma \tilde{S} \right] &= 0 \\ \left[ \frac{\delta}{\delta t} + v \frac{\delta}{\delta x} \right] \left[ \tilde{S} \right] &= 0 \end{aligned} \right\} \quad (3)$$

The solutions of equations (3) may be written in terms of the Laplace transform operator  $s$  as:

$$\left. \begin{aligned} \left[ \tilde{P}_{n+1} + \alpha \tilde{w}_{n+1} + \beta \tilde{S}_{n+1} \right] &= e^{-\sigma s} \left[ \tilde{P}_n + \alpha \tilde{w}_n + \beta \tilde{S}_n \right] \\ \left[ \tilde{P}_{n+1} - \alpha \tilde{w}_{n+1} - \gamma \tilde{S}_{n+1} \right] &= e^{+\sigma s} \left[ \tilde{P}_n - \alpha \tilde{w}_n - \gamma \tilde{S}_n \right] \\ \left[ \tilde{S}_{n+1} \right] &= e^{-\theta s} \left[ \tilde{S}_n \right] \end{aligned} \right\} \quad (4)$$

where  $\sigma = L/(v+a)$ ,  $\tau = L/(a-v)$ , and  $\theta = L/v$  and  $L$  is the linear distance between stations  $n$  and  $(n+1)$ . The integration performed between equations (3) and (4) is only valid for a constant area duct. The variable area portion of the subsonic diffuser is assumed to be made up of three constant area sections. The boundary conditions between the sections pose no problem since total pressure, flow and entropy may be regarded as constant across the interface.

Equations (1) and (4) when combined with appropriate terminal conditions for the subsonic duct and disturbance equations written in terms of the selected variables, provide a mathematical model which can be applied to a mixed compression inlet.

In the mathematical analysis of Ref. 2, the effects of performance bleed were not considered. For the test data here presented, however, it is necessary to include the performance bleed. If perturbations in upstream flow are included in the second of equations (1), it becomes:

$$\frac{\Delta \dot{w}_2}{\dot{w}} = \frac{\Delta \dot{w}_1}{\dot{w}} + C_3 s \frac{\Delta X_s}{L_T} \quad (5)$$

Figure 8 shows a normal shock standing in a region with performance bleeds. In this figure stations 1 and 2 are just beyond the range of normal shock travel, while stations 1a and 2a are adjacent to the normal shock in the bleed region. With the nomenclature of this figure, equation (5) becomes:

$$\frac{\Delta \dot{w}_{2a}}{\dot{w}} = \frac{\Delta \dot{w}_{1a}}{\dot{w}} + C_3 s \frac{\Delta X_s}{L_T} \quad (6)$$

The flow at station 1 is related to that at station 1a by

$$\dot{w}_1 = \dot{w}_{1a} + \dot{w}_{1b}$$

or

$$\frac{\Delta \dot{w}_1}{\dot{w}} = \frac{\Delta \dot{w}_{1a}}{\dot{w}} + \frac{\Delta \dot{w}_{1b}}{\dot{w}} \quad (7)$$

where  $\dot{w}_{1b}$  is the bleed flow between stations 1 and 1a. Similarly:

$$\frac{\Delta \dot{w}_2}{\dot{w}} = \frac{\Delta \dot{w}_{2a}}{\dot{w}} - \frac{\Delta \dot{w}_{2b}}{\dot{w}} \quad (8)$$

If the effects of small perturbations in pressure are neglected, the bleed flows are proportional to shock position.

$$\dot{w}_{1b} = \bar{w}_{1b} + K_{1b} \frac{\Delta X_s}{L_T}$$

or

$$\Delta \dot{w}_{1b} = K_{1b} \frac{\Delta X_s}{L_T} \quad (9)$$

and

$$\Delta \dot{w}_{2b} = -K_{2b} \frac{\Delta X_s}{L_T} \quad (10)$$

Substituting into equation (6) results in

$$\frac{\Delta \dot{w}_2}{\dot{w}} - \frac{\Delta \dot{w}_1}{\dot{w}} = (K_{2b} - K_{1b}) \frac{\Delta X_s}{L_T} + C_3 s \frac{\Delta X_s}{L_T}$$

or neglecting upstream disturbances

$$\tilde{w} = (C_B + C_3 s) \tilde{X}_s \quad (11)$$

Steady state test data obtained for the performance bleed flow as a function of shock position indicates the linear relation predicted by equation (11).

In the actual application of the analytical technique to a real problem, the principal difficulty arises in determining the appropriate value of  $A'/A$  (i.e.,  $1/A \, dA/dx$  in the vicinity of the normal shock). Because of boundary layer effects, the actual geometric value does not give satisfactory results. It was found empirically that  $A'/A = 0.013/\text{cm}$  gave good agreement for the low frequency gain and fair frequency response agreement. This value was thus used in all of the analytical data presented. The bleed coefficient ( $0.00151/\text{cm}$ ) was based on actual experimental data. Although the curves presented show fair correlation between experiment and theory, the results could be improved by better selection of these two parameters.

Figure 9 presents shock position frequency response obtained for the experimental inlet with the long cold pipe attached. Both the test data and the analytical results exhibit the repeated resonances typical of a distributed parameter system.

Figures 10 and 11 present frequency response data for shock position and static pressure just downstream of the shock. These two figures are also for the experimental inlet, but with the cold pipe replaced by a choked station at the end of the variable area portion of the duct. In both plots the phase agreement is good but although the analytical results exhibit a plateau in the amplitude ratio plots they fail to exhibit the distinct resonance of the test data. One possible source of the discrepancy arises from the fact that the actual disturbance device is separated from the inlet duct by a volume. This volume has not been included in the analytical model.

### Concluding Remarks

Dynamic response of the shock position resulting from a symmetrical internal disturbance showed that:

1. Resonance was observed at about 55 Hz.
2. Little or no change in the resonant frequency was observed when the internal flow choke points were changed or when the engine was coupled to the inlet.
3. The dynamic response of the shock position was observed to be similar for the compressor face choke point and inlet-engine configurations.
4. The additional volume of the inlet configuration with the internal flow choked at the model exit resulted in a more rapid decrease in amplitude ratio.
5. Sealing the downstream throat bleed resulted in increased sensitivity of the terminal shock to downstream disturbances.
6. Dynamic response of the shock position to an external disturbance was nonresonant over the test frequency range for the inlet-engine configuration.
7. Comparison of the analytical and the experimental data indicates that fair agreement can be achieved between the two. Further work should include the effects of the volume associated with the disturbance device. In addition, a finer lumping of the diverging portion of the subsonic diffuser should be investigated to determine the effects on accuracy.

### Symbols

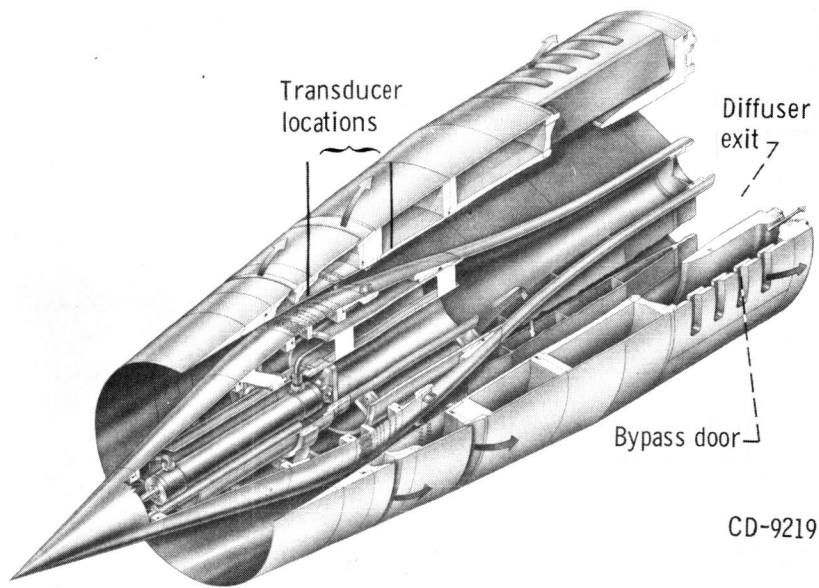
A	area
A'	dA/dx
a	speed of sound
C <sub>B</sub>	bleed flow coefficient
C <sub>1</sub> , C <sub>2</sub> , C <sub>3</sub>	coefficients with appropriate dimensions
g	acceleration due to gravity
K <sub>1b</sub> , K <sub>2b</sub>	bleed flow coefficients
L	length
M	Mach number
n	station number
P	pressure
R	universal gas constant
S	entropy
s	Laplace transform operator
t	time
v	velocity
w	flow rate

X <sub>S</sub>	shock position
x	space coordinate
$\alpha, \beta, \gamma$	functions of Mach number defined in text
$\rho$	density
$\sigma, \tau, \theta$	delay times
$\varphi$	gust plate angle of attack

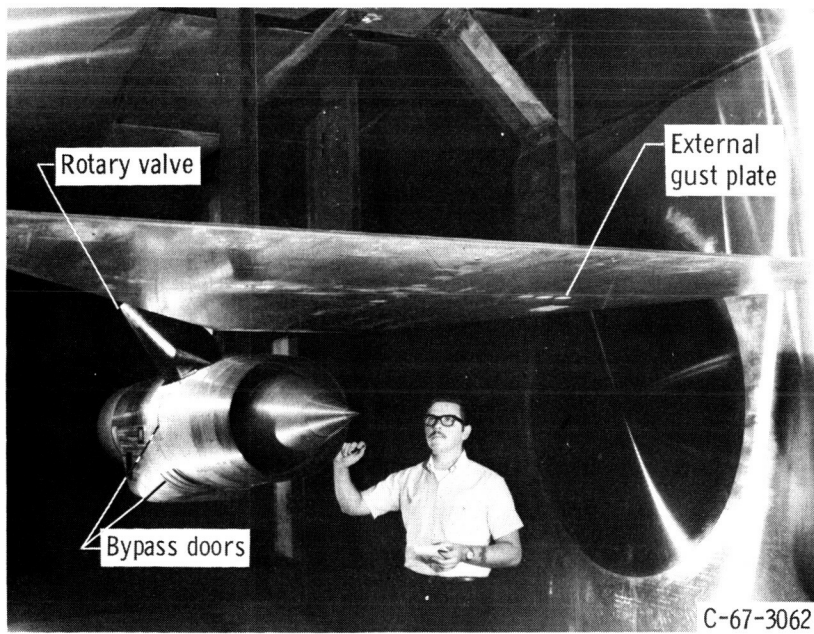
The subscript T denotes total conditions. A bar over a variable denotes the steady state value of the variable. The symbol  $\Delta$  preceding a variable denotes a small perturbation quantity. In general, numerical subscripts denote the station associated with the variable as defined in Fig. 8.

### References

1. Wasserbauer, J. F. and Whipple, D. L., "Dynamic Response of a Supersonic Diffuser to External and Internal Disturbances," Proposed NASA Technical Memorandum.
2. Willoh, R. G., "A Mathematical Analysis of Supersonic Inlet Dynamics," Proposed NASA Technical Memorandum.
3. Cubbison, R. W., Meleason, E. T., and Johnson, D. F., "Effect of Amount and Location of Porous Bleed in a High Performance Axi-Symmetric Mixed Compression Inlet at Mach 2.5." Proposed NASA Technical Memorandum.
4. Bowditch, D. N. and Wilcox, F. A., "Dynamic Response of a Supersonic Diffuser to Bypass and Spike Oscillation." TM X-10, 1959, National Aeronautics and Space Administration, Cleveland, Ohio.
5. Walitt, L., "On the Dynamics of a Supercritical Inlet," M. S. Thesis, 1962, Univ. California, Los Angeles.



(a) Isometric view.



(b) Photograph of inlet model.

Figure 1. - Experimental inlet model.

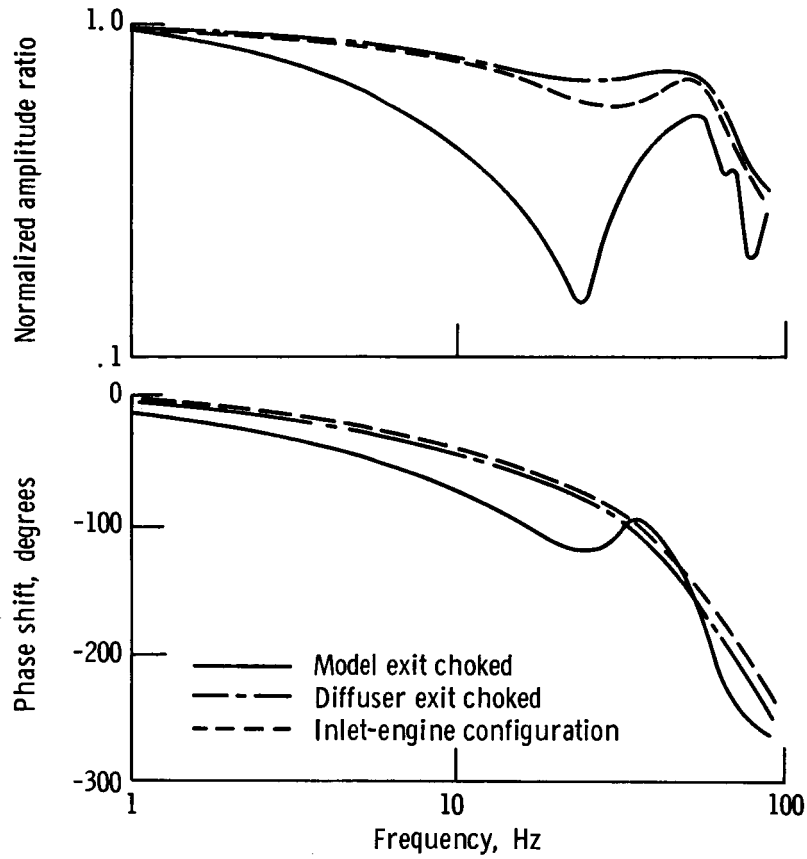


Figure 2. - Dynamic response of shock position to symmetrical internal disturbance.

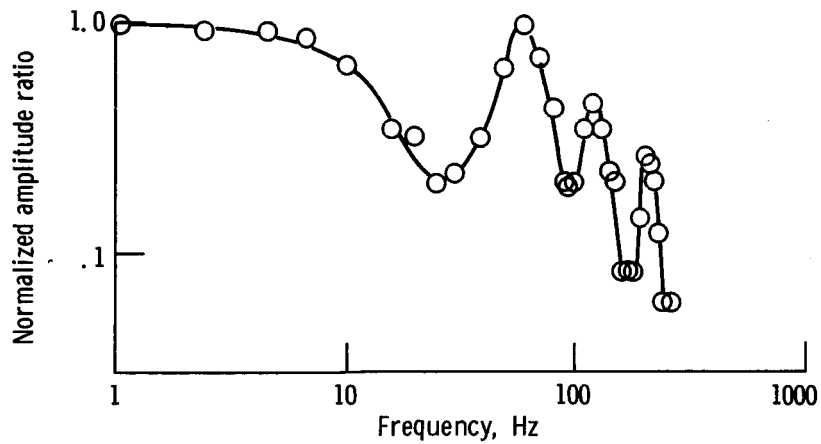


Figure 3. - Dynamic response of shock position to unsymmetrical internal disturbance. Model exit choked; inlet unstart method.

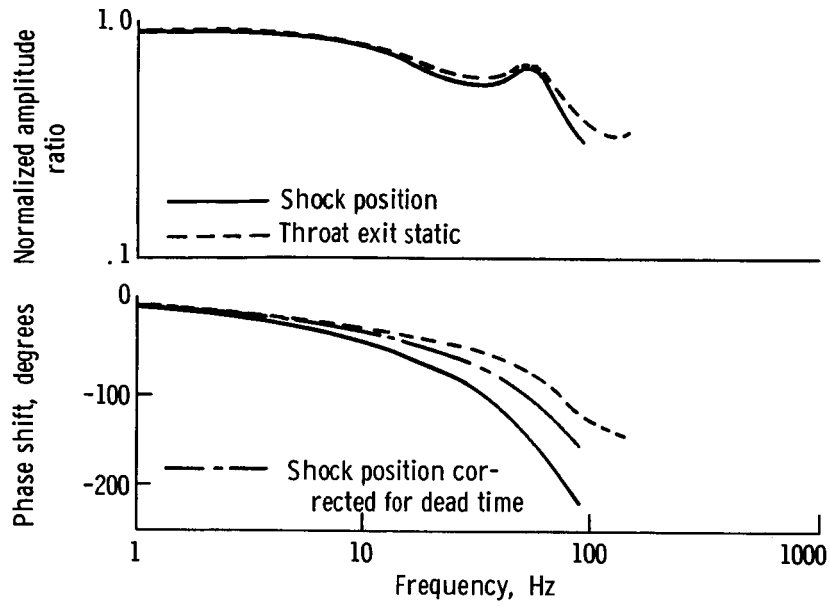


Figure 4. - Response of shock position and throat exit static pressure; inlet-engine configuration.

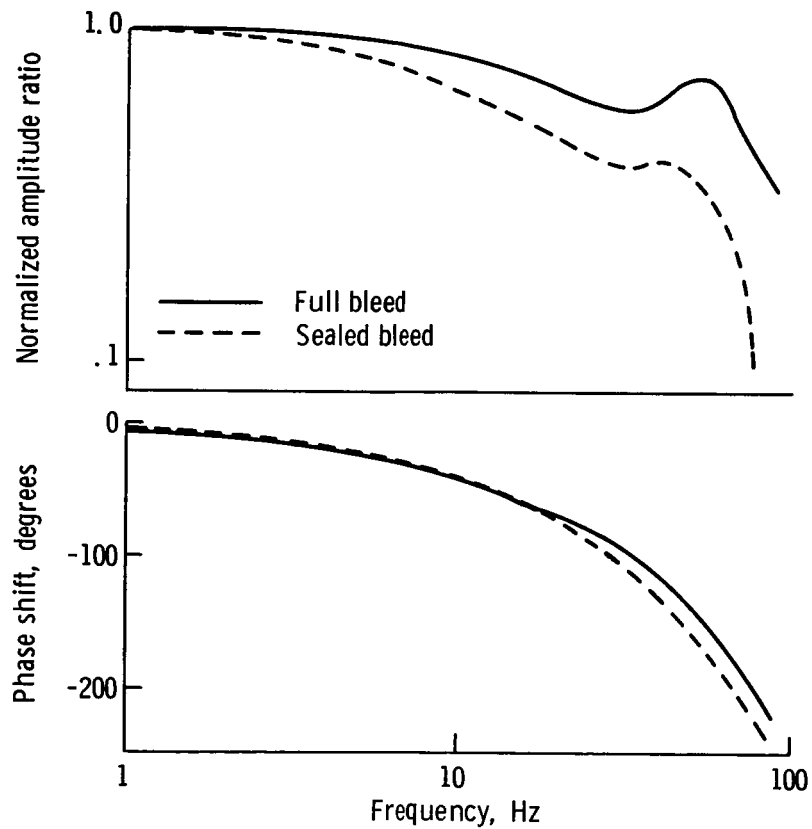


Figure 5. - Effect of inlet throat bleed on shock position dynamics; inlet-engine configuration.

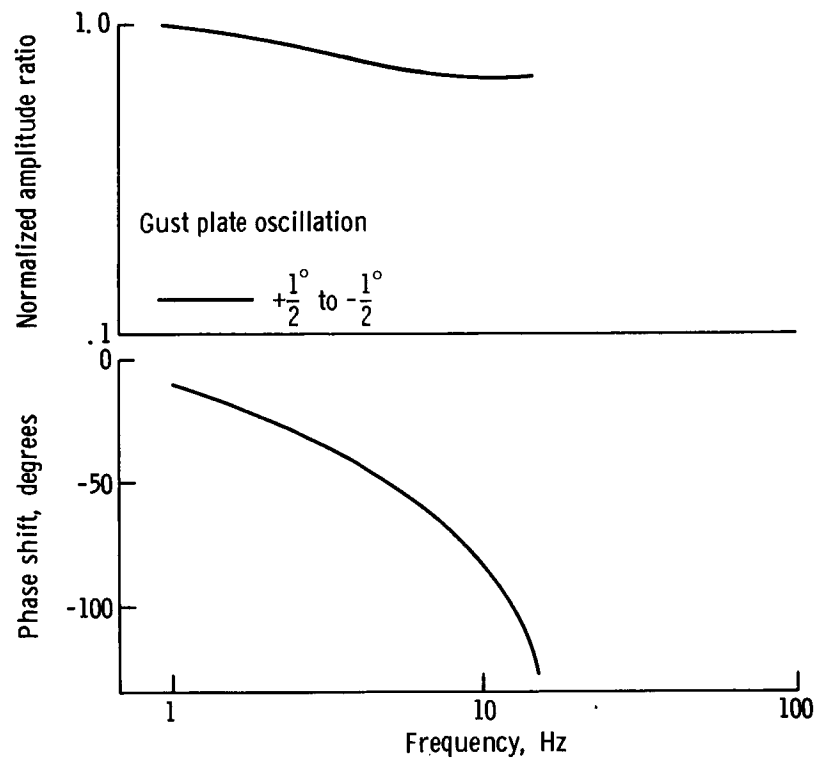


Figure 6. - Shock position response to external disturbance. Inlet-engine configuration; throat bleed sealed.

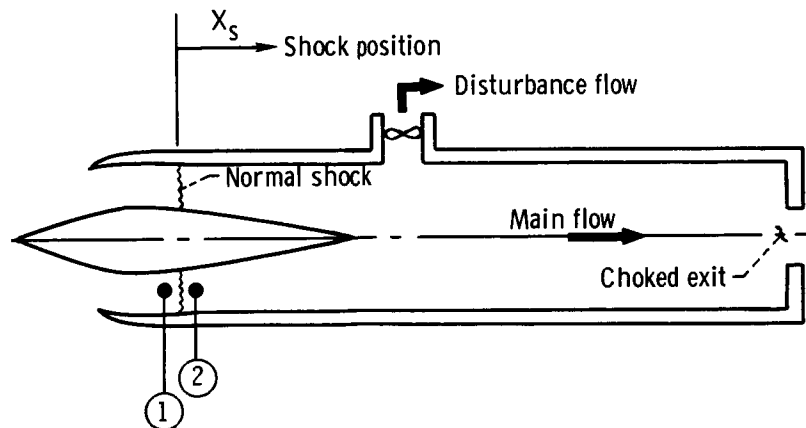


Figure 7. - Idealized inlet.

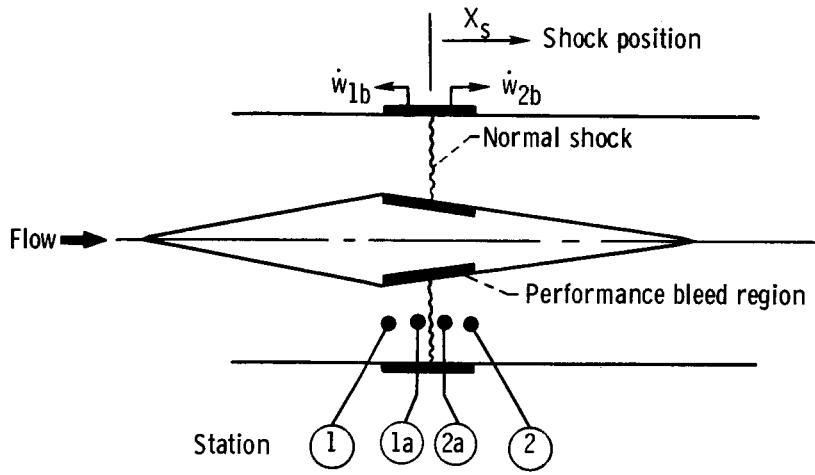


Figure 8. - Performance bleed schematic.

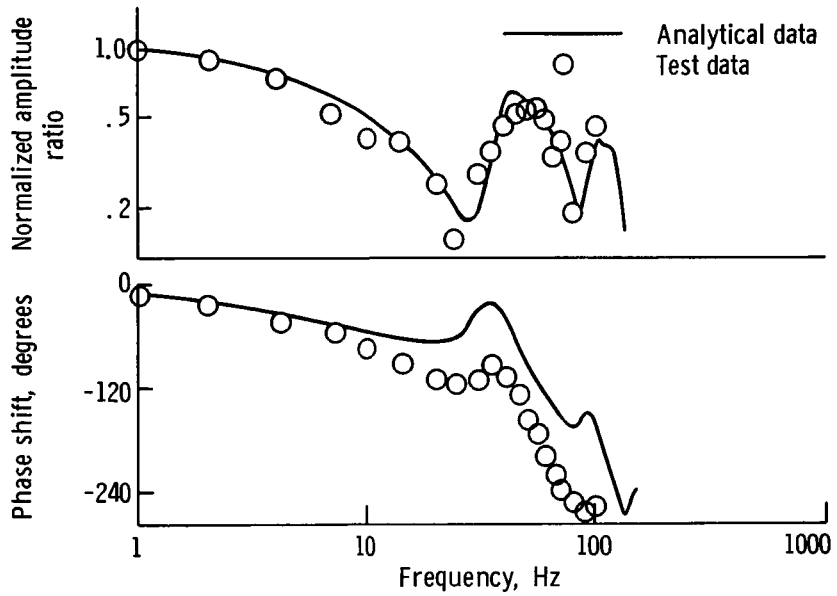


Figure 9. - Response of shock position to flow disturbance for inlet with model exit choked.

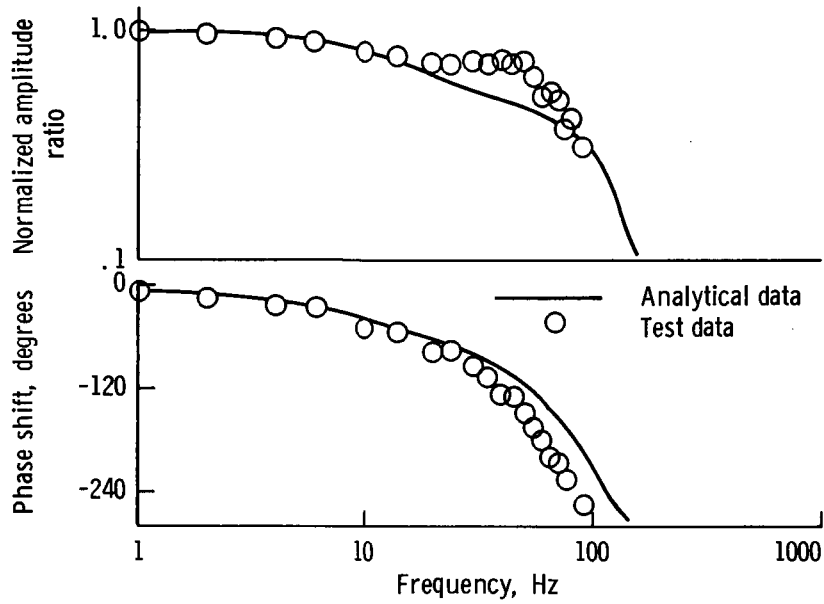


Figure 10. - Response of shock position to flow disturbance for inlet with diffuser exit choked.

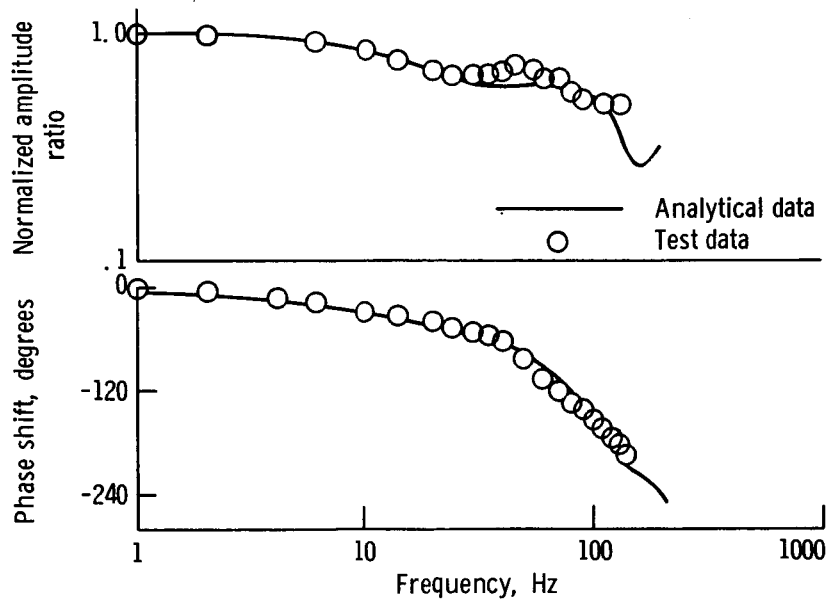


Figure 11. - Response of throat exit static pressure to flow disturbance for inlet with diffuser exit choked.